

Direct Observation of Charge Order in Triangular Metallic AgNiO_2 by Single-Crystal Resonant X-Ray Scattering

G. L. Pascut,^{1,2} R. Coldea,¹ P. G. Radaelli,¹ A. Bombardi,³ G. Beutier,³ I. I. Mazin,⁴ M. D. Johannes,⁴ and M. Jansen⁵

¹*Clarendon Laboratory, University of Oxford, Parks Road, Oxford OX1 3PU, United Kingdom*

²*H. H. Wills Physics Laboratory, University of Bristol, Tyndall Avenue, Bristol, BS8 1TL, United Kingdom*

³*Diamond Light Source Ltd., Harwell Science and Innovation Campus, Didcot, Oxfordshire, OX11 0DE, United Kingdom*

⁴*Code 6393, Naval Research Laboratory, Washington, D.C. 20375, USA*

⁵*Max-Planck Institut für Festkörperforschung, Heisenbergstrasse 1, D-70569 Stuttgart, Germany*

(Received 10 September 2010; published 13 April 2011)

We report resonant x-ray scattering measurements on a single crystal of the orbitally degenerate triangular metallic antiferromagnet $2H\text{-AgNiO}_2$ to probe the spontaneous transition to a triple-cell superstructure at temperatures below $T_S = 365$ K. We observe a strong resonant enhancement of the supercell reflections through the Ni K edge. The empirically extracted K -edge shift between the crystallographically distinct Ni sites of 2.5(3) eV is much larger than the value expected from the shift in final states, and implies a core-level shift of ~ 1 eV, thus providing direct evidence for the onset of spontaneous honeycomb charge order in the triangular Ni layers. We also provide band-structure calculations that explain quantitatively the observed edge shifts in terms of changes in the Ni electronic energy levels due to charge order and hybridization with the surrounding oxygens.

DOI: 10.1103/PhysRevLett.106.157206

PACS numbers: 75.25.Dk, 71.45.Lr, 78.70.Ck

Since the discovery of the Verwey transition in 1939 [1], electronic ordering in oxides has been extensively studied, as more evidence progressively emerged of its importance in underpinning phenomena such as metal-insulator transitions, colossal magnetoresistance, and possibly high-temperature superconductivity. Orbital ordering (OO), in particular, whereby orbital degeneracy is lifted either by a spontaneous lattice distortion driven by the (cooperative) Jahn-Teller (JT) effect [2], or by similar orbital physics [3], has become a cornerstone of our understanding of oxides. This was hitherto considered ubiquitous in both band and Mott insulators containing “JT-active” ions. For this reason, the recent proposal [4] of a radically different type of electronic ordering in the weakly metallic $2H\text{-AgNiO}_2$ came initially as a surprise. In this scenario, orbital degeneracy at JT-active low-spin Ni^{3+} would be lifted through charge disproportionation and charge ordering (CO) rather than OO, in sharp contrast with the closely related (but insulating) nickelate NaNiO_2 [5], a rather conventional JT system. Although CO was observed before, e.g., at the metal-insulator transition in rare-earth perovskite nickelates [6,7], elucidating the physics of $2H\text{-AgNiO}_2$ is crucial in establishing CO as an alternative paradigm to the Jahn-Teller mechanism in “weakly” metallic systems close to the Mott transition [4,8], which remain metallic in the CO state. Furthermore, the “pure” CO (without magnetic order [9]) exists over a wide temperature range $T_N < T < T_S = 365$ K, with magnetic order occurring only below $T_N = 19.7$ K. The first indication for CO in $2H\text{-AgNiO}_2$ was structural, and relied on an accurate neutron refinement of an oxygen breathing mode around the different Ni sites [Fig. 1(b)] in the $\sqrt{3}a_0 \times \sqrt{3}a_0 \times c$ supercell

structure at $T < T_S$, which suggested a “honeycomb” CO pattern [Fig. 1(a)]. A substantial amount of charge disproportionation is suggested by a bond valence sum analysis [10] of the Ni-O bond lengths, which yields $\text{Ni}1^{2.42+}$ and $\text{Ni}2, 3^{3.07+}$.

Here we present resonant Ni- K -edge x-ray scattering data on a single crystal of $2H\text{-AgNiO}_2$ to probe directly the electronic order at the Ni sites. This technique has been widely employed in the past to explore charge and orbital order [11] because of its sensitivity to subtle differences in

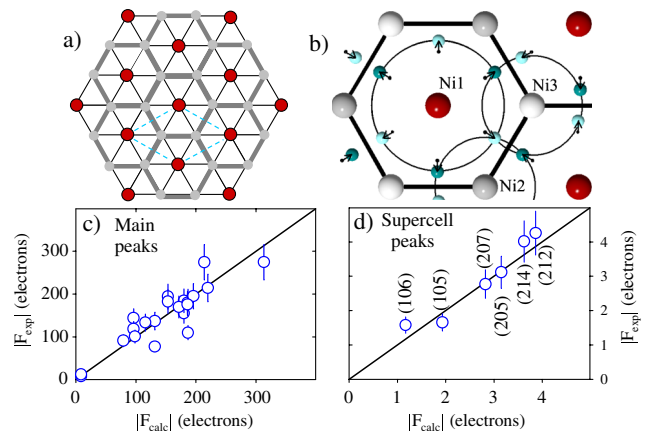


FIG. 1 (color online). (a) Schematic of the honeycomb CO in the triangular lattice: red (dark) balls are electron-rich Ni1 sites nested inside a honeycomb (thick contour) of electron-depleted Ni2,3 sites (gray balls). The dashed rhombus is the CO supercell. (b) Oxygen breathing mode around electron-rich and electron-depleted Ni sites. (c),(d) Observed versus calculated off-resonance (8.3 keV) $|F|$ for main and supercell peaks.

the electronic configuration. In particular, Ni K -edge resonant scattering probes primarily dipole-allowed transitions from the core $1s$ levels, which shift in response to the amount of charge on the ion, to the empty $4p$ band, which is strongly sensitive to changes in the coordination environment. From our data we extract in an unbiased way the anomalous scattering factors of the different Ni sites. By comparing the experimental results with band-structure calculations, we show that the $4p$ level shift accounts for just over half of the edge shift, implying a core-level shift of ~ 1 eV that provides direct evidence of honeycomb CO. We also show that the results are quantitatively consistent with the amount of charge disproportionation predicted by local-density approximation (LDA) calculations.

Our sample was a small single-crystal platelet of $2H\text{-AgNiO}_2$ of diameter ~ 70 μm in the ab plane and thickness ~ 20 μm , extracted from a polycrystalline batch [12]. A full single-crystal x-ray diffraction pattern collected at 300 K using an Oxford Diffraction Mo-source diffractometer confirmed the hexagonal unit cell found previously [space group $P6_322$ with $a = b = \sqrt{3}a_0 = 5.0908(1)$ \AA , $c = 12.2498(1)$ \AA] where supercell peaks are indexed by (h, k, l) with $h - k = 3n + 1$ or $3n + 2$ and correspond to the oxygen breathing order pattern shown in Fig. 1(b). Synchrotron resonant x-ray diffraction was performed at the Diamond Light Source in Didcot, UK, on beam line I16 operated with a Si (111) double-crystal monochromator ($\Delta E/E \approx 10^{-4}$ at 8.35 keV). The azimuth of each supercell reflection was chosen such that the incident polarization lay close to the ab plane of the crystal (see later). The sample temperature was controlled via a nitrogen gas flow. Intensities were collected by a 2D Pilatus detector, and a typical intensity map for a supercell Bragg reflection is shown in Fig. 2, top-left inset. Total peak intensities were extracted by integrating the counts over rocking-curve scans around the peak position. After all corrections [13], the off-resonance structure factors $|F|$ at 300 K for all measured main peaks, as well as supercell peaks, agreed very well with the calculated values, see Figs. 1(c) and 1(d), enabling us to convert scattering intensities into $|F|^2$ in absolute units.

Figure 2 shows the energy-dependent $|F|^2$ for three supercell reflections (out of the 6 measured), which are representative of the different types of resonant responses. In particular, the (109) peak is entirely due to anomalous scattering from Ni as it is practically absent off resonance. The middle and bottom panels show the (105) and (205) supercell peaks, which have a sizable oxygen contribution, as evidenced by the preedge scattering.

In the dipolar approximation the atomic scattering factor near the K -edge absorption energy E_A is

$$f(Q, E) = f^0(Q) + f'(E) + if''(E), \quad (1)$$

where f^0 is the conventional (Thomson) Q -dependent scattering factor [15] and f' , f'' are the real and imaginary

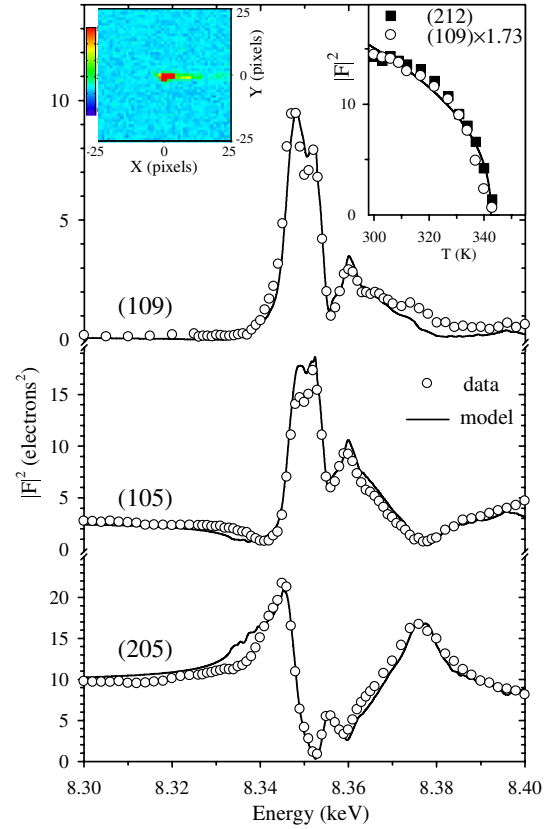


FIG. 2 (color online). Energy-dependent intensity of three supercell reflections at 300 K near the Ni K edge [solid lines are model calculations using Eq. (2)]. Top-left inset: Example of raw 2D pixelated area detector data for (109) near resonance. The horizontal (vertical) angular coverage is $\approx 1^\circ$ (0.7°). Top-right inset: Temperature dependence of peak intensities near resonance (8.347 keV) for (109), dominated by Ni charge order (open symbols, scaled) and for (212), with contributions from both Ni CO and oxygen displacements (solid squares). Solid line is a guide to the eye. The transition temperature is offset with respect to the specific heat [4] [343(1) vs 365(5) K], probably due to x-ray beam heating effects.

parts of the anomalous scattering factor, respectively. In essence, the rich structures observed in Fig. 2 are due to the fact that E_A of the electron-rich Ni1 is slightly different from that of electron-depleted Ni2,3 providing a strong energy-dependent contrast between the two sites. For the peaks in Fig. 2 the $|F|^2$ is

$$|F(Q, E)|^2 = 3[\mp A_Q f_O^0 + \Delta f_{\text{Ni}}^0 + \Delta f_{\text{Ni}}^l]^2 + 3\Delta f_{\text{Ni}}^{l2}, \quad (2)$$

where the upper sign applies for (109) and (105) and lower sign for (205). The dominant term off resonance is $A_Q f_O^0$, the energy-independent structure factor [16] for the oxygen breathing displacement order, which is weak for (109) and strong for (205) and (105). In contrast, the terms $\Delta f_{\text{Ni}}^l = f_{\text{Ni1}}^l(E) - f_{\text{Ni3}}^l(E)$ and $\Delta f_{\text{Ni}}^{l2} = f_{\text{Ni1}}^{l2}(E) - f_{\text{Ni3}}^{l2}(E)$ have the same value for different reflections but are strongly energy dependent and are due to the contrast between the

anomalous atomic factors for Ni1 inside the honeycomb and Ni3 on the honeycomb (contributions from Ni2 cancel by symmetry). The remaining term $\Delta f_{\text{Ni}}^0 = f_{\text{Ni1}}^0 - f_{\text{Ni3}}^0$ is the Thomson charge contrast. All contributions to Eq. (2) cancel in the high-temperature phase above T_S , since all Ni sites become equivalent and the oxygens are not displaced from their ideal positions. This can be shown by plotting the intensity of different superlattice reflections as a function of temperature (top-right inset of Fig. 2). These data also show that the order parameter obtained from the purely resonant peak (109) (“CO order parameter”) is essentially the same as extracted from the intensity of the (212) supercell peak, which has comparable contributions from both Ni CO and oxygen displacements, indicating that, as expected, CO and displacements are strongly coupled and both go to zero together at T_S .

It is important to point out that, because of the asphericity of the electron density, f' and f'' in Eq. (1) are in general not scalar quantities, but depend on the orientation of the incident and scattered polarizations with respect to the crystallographic axes, as expressed through the general tensor relation $\hat{f}(E) = \sum_{\alpha,\beta} f^{\alpha\beta} \epsilon_\alpha \epsilon'_\beta$ (valid for both f' and f''), where ϵ and ϵ' are the incident and scattered polarization vectors. In $2H\text{-AgNiO}_2$ the local threefold symmetry axis at each Ni site restricts \hat{f}' and \hat{f}'' to have a diagonal form in the orthogonal reference frame xyz where $x \parallel a$ and $z \parallel c$, such that $\hat{f} = [f_\perp \ 0 \ 0; 0 \ f_\perp \ 0; 0 \ 0 \ f_\parallel]$, where \parallel is along the c axis and \perp is in the ab plane. Because of our choice of azimuth, the incident polarization was always nearly perpendicular to the c axis. Consequently, our data were sensitive only to $\sigma\sigma$ -type scattering [17] and we can employ the scalar relation in Eq. (2) with f' and f'' being the in-plane components f'_\perp and f''_\perp of the anomalous scattering tensors.

Remarkably, the complex multiple-peak structure of the spectra in Fig. 2 can be reproduced quantitatively (in absolute units) by a model (solid lines) based on an unbiased reconstruction of the atomic scattering factors for the Ni1 and Ni2,3 [Fig. 3(b)]. In this analysis we assumed identical scattering factors for both Ni sites on the honeycomb $f_{\text{Ni2}} = f_{\text{Ni3}}$ as their first-neighbor environments (Ni-O bond lengths and angles) are identical [4]. The two functions $f''_{\text{Ni1}}(E)$ and $f''_{\text{Ni3}}(E)$ were optimized iteratively to best match the observed spectra, under the constraints of a given average $f''_{\text{fu}} = f''_{\text{Ag}}(E) + 2f''_{\text{O}}(E) + [f''_{\text{Ni1}}(E) + 2f''_{\text{Ni3}}(E)]/3$ per formula unit, which is related to the linear absorption coefficient via [14] $\mu(E) = (2Zhc r_e / V_{\text{uc}} E) f''_{\text{fu}}(E)$, where $Z = 6$ is the number of formula units per unit cell of volume V_{uc} , hc/E is the x-ray wavelength, and r_e is the classical electron radius. The real parts of the scattering factors f' in Eq. (2) were obtained via the Kramers-Kronig (KK) relation [14,18] from the imaginary parts f'' , such that the individual anomalous scattering factors obey the KK relation. Starting values for the profiles $f''_{\text{Ni1,3}}(E)$ were obtained by subtracting the intensities

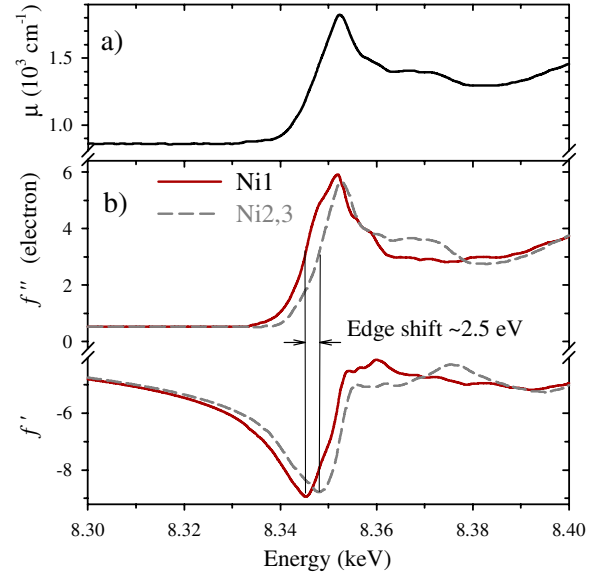


FIG. 3 (color online). (a) Absorption coefficient $\mu(E)$ obtained from transmission data. (b) Energy dependence of the empirically extracted real and imaginary parts of the anomalous atomic scattering factors for Ni1 (solid line) and Ni2,3 (dashed line) obtained from the best fit to the data in Fig. 2.

$|F(\mathbf{Q}, E)|^2$ such as in Fig. 2 for various reflections (with the energy-independent terms $\mp A_{\mathbf{Q}} f_{\text{O}}^0 + \Delta f_{\text{Ni}}^0$ replaced by their measured values off resonance) to give the difference $f'_{\text{Ni1}}(E) - f'_{\text{Ni3}}(E)$. After inserting this back into Eq. (2) one obtains the modulus $|f''_{\text{Ni1}}(E) - f''_{\text{Ni3}}(E)|$. Combining this with the constraint for the sum $f''_{\text{Ni1}}(E) + 2f''_{\text{Ni3}}(E)$ yields a few possibilities for starting profiles for the two functions $f''_{\text{Ni1,3}}(E)$ (this is due to the sign uncertainty), but with only one set satisfying all the constraints above. The best parametrization of the data (solid lines in Fig. 2) is obtained for the atomic scattering factors in Fig. 3(b), which show a clear energy shift of the edge of +2.5(3) eV and some subtle differences at higher energy [19]. The sign of the energy shift is fully consistent with an electron-rich Ni1 site [20,21] and is uniquely determined from the data. In addition, the absolute scaling of the peak intensities ensures an accurate and reliable determination of the magnitude of the edge shift.

Edge shifts are often taken as directly proportional to changes in the formal valence of the ion. For octahedral Ni, the proportionality constant is $\sim 0.66 e/\text{eV}$ [20], so an edge shift of 2.5 eV corresponds to a disproportionation of ~ 1.65 electrons, in very good agreement with the expected CO scenario of Ni1^{2+} and $\text{Ni2,3}^{3.5+}$ [4]. However, the initial- and final-state contributions to the edge shift are typically of similar magnitudes, while only the former are directly related to charge ordering. To estimate the core-level shifts, we determined the positions of the $4p$ final states from LDA band-structure calculations [4]. The $4p_{x,y}$ (degenerate) densities of states are shown in Fig. 4 (only these bands are probed in the present

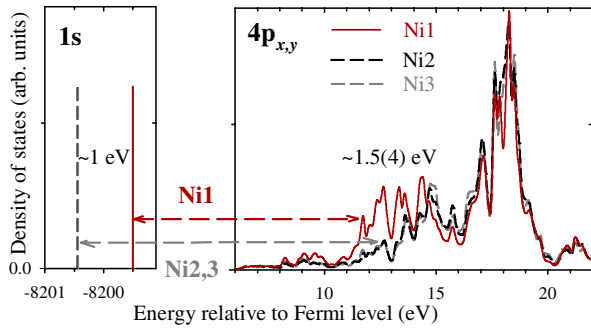


FIG. 4 (color online). LDA calculation of density of states (DOS) for the initial and final electron states in the transition $1s \rightarrow 4p_{x,y}$ (horizontal dashed arrows) probed by the present resonant Ni K -edge scattering experiments. Solid (dashed) curves show the DOS for electron-rich (electron-depleted) Ni1 (Ni2,3) sites. The combined effect is a predicted transition energy shift of 2.5(4) eV higher for Ni2,3 compared to Ni1, in excellent agreement with the experiment.

experiments [17]). The Ni1 and Ni2,3 $4p$ bands are shifted by ~ 1.5 eV, well short of the 2.5(3) eV observed experimentally, providing clear evidence that a core-level shift of ~ 1 eV is required to reproduce the data. Further insight can be gained by extracting directly the positions of the core $1s$ levels on the Ni1 and Ni2,3 sites from the LDA calculations (left panel, Fig. 4), which indeed differ by ~ 1 eV. This demonstrates that LDA calculations are quantitatively consistent with the resonant scattering experiments, and provides strong evidence of honeycomb CO with an amount of charge disproportionation in agreement with LDA.

In summary, we have reported Ni- K -edge resonant x-ray scattering measurements on the orbitally degenerate metal $2H$ - AgNiO_2 to investigate the transition to a tripled hexagonal unit cell. We have observed a large resonant effect on the superstructure reflections with a rich energy-dependent structure that can be quantitatively accounted for by interference scattering from the electron-rich and electron-depleted Ni sites with energy-shifted atomic scattering factors. By considering the various contributions to this edge shift we have determined a core-level shift of ~ 1 eV between Ni sites, in quantitative agreement with first principles electronic structure calculations, thus providing clear, direct, and quantitative evidence of charge order in the triangular Ni layers. Charge order as an alternative to orbital ordering in systems with Jahn-Teller active ions was recently brought into the spotlight in connection with 3D perovskite nickelates $R\text{NiO}_3$ [8], and is likely controlling the essential physics of ferrates CaFeO_3 [22] and $\text{Sr}_3\text{Fe}_2\text{O}_7$ [23] and other orbitally degenerate systems located in the crossover region between local Mott insulator and itinerant behavior.

We acknowledge support from EPSRC UK and a studentship from the University of Bristol and Harold Herbert Potter Fund (G. L. P.). We thank E. Wawrzyńska and M.

Brunelli for characterizing the polycrystalline sample on Beamline ID31 at the ESRF.

- [1] E. J. W. Verwey, *Nature (London)* **144**, 327 (1939).
- [2] H. Jahn and E. Teller, *Proc. R. Soc. A* **161**, 220 (1937).
- [3] K. I. Kugel and D. I. Khomskii, *Sov. Phys. Usp.* **25**, 231 (1982).
- [4] E. Wawrzyńska *et al.*, *Phys. Rev. Lett.* **99**, 157204 (2007); *Phys. Rev. B* **77**, 094439 (2008).
- [5] E. Chappel *et al.*, *Eur. Phys. J. B* **17**, 615 (2000).
- [6] J. A. Alonso *et al.*, *Phys. Rev. Lett.* **82**, 3871 (1999).
- [7] U. Staub *et al.*, *Phys. Rev. Lett.* **88**, 126402 (2002).
- [8] I. I. Mazin *et al.*, *Phys. Rev. Lett.* **98**, 176406 (2007).
- [9] S. B. Lee, R. Chen, and L. Balents, *Phys. Rev. Lett.* **106**, 016405 (2011).
- [10] I. D. Brown, in *Structure and Bonding in Crystals*, edited by M. O'Keefe and A. Navrotsky (Academic, New York, 1981), Vol. 2, p. 130.
- [11] Y. Murakami *et al.*, *Phys. Rev. Lett.* **80**, 1932 (1998).
- [12] T. Sörgel and M. Jansen, *Z. Anorg. Allg. Chem.* **631**, 2970 (2005); *J. Solid State Chem.* **180**, 8 (2007).
- [13] Raw intensities were corrected for Lorentz factor, Debye-Waller factor [12], and absorption using a beam-path integration routine for a disk-shaped sample with effective dimensions refined against measured (off-resonance) intensity ratios of several main (hkl) reflections with $h - k = 3n$ and l odd for which Ni contributions to F cancel out. $\mu(E)$ was extracted from the measured transmission spectrum through a thin layer of powder distributed on kapton tape. The numerical approximation [14] for $f'(E)$ and $f''(E)$ was used off resonance.
- [14] C. T. Chantler, *J. Phys. Chem. Ref. Data* **24**, 71 (1995).
- [15] *International Tables for Crystallography*, edited by A. J. C. Wilson (Kluwer, Dordrecht, 1992), Vol. C, pp. 182 and 500.
- [16] $A_{(h0l)}\sqrt{3} = 4 \sin(2\pi lz)\{\sin[2\pi h(x - y)] + \sin(2\pi hy) - \sin(2\pi hx)\}$, $x = 1/3$, $y = 0.0133$, $z = 1/4 + 0.0805$.
- [17] For the case of no analyzer (as in the present experiments) Eq. (2) becomes the sum (we drop the E and Q dependence for brevity) $|F|^2 = |F|_{\sigma\sigma}^2 + |F|_{\sigma\pi}^2$, where $|F|_{\sigma\sigma}^2 = 3[\mp A_Q f_0^0 + \Delta f_0^0 + \Delta f_{\perp}^0 + \gamma^2(\Delta f_{\parallel}^0 - \Delta f_{\perp}^0)]^2 + 3[\Delta f_{\parallel}^0 + \gamma^2(\Delta f_{\parallel}^0 - \Delta f_{\perp}^0)]^2$ and $|F|_{\sigma\pi}^2 = 3(\gamma\gamma')^2[(\Delta f_{\parallel}^0 - \Delta f_{\perp}^0)^2 + (\Delta f_{\parallel}^0 - \Delta f_{\perp}^0)^2]$, where the difference terms are $\Delta f_{\perp}^0 = f_{\perp}^0(\text{Ni1}) - f_{\perp}^0(\text{Ni3})$ and so on. Here γ , γ' are projections onto the crystal c^* axis of the incident x-ray beam polarization vector σ (which is perpendicular to the scattering plane) and of the vector π (within the scattering plane and \perp to k_f).
- [18] I. J. Pickering *et al.*, *J. Am. Chem. Soc.* **115**, 6302 (1993).
- [19] The assumption $f_{\text{Ni2}} = f_{\text{Ni3}}$ was further justified by the observed agreement with the data at supercell peaks with l even, (106), where both Ni2 and Ni3 contribute.
- [20] A. N. Mansour and C. A. Melendres, *J. Phys. Chem. A* **102**, 65 (1998); *J. Phys. IV* **7**, C2-1171 (1997).
- [21] T. A. Carlson, in *Photoelectron and Auger Spectroscopy* (Plenum, New York, 1975), p. 165.
- [22] M. Takano *et al.*, *Mater. Res. Bull.* **12**, 923 (1977).
- [23] K. Kuzushita *et al.*, *J. Phys. Soc. Jpn.* **69**, 2767 (2000).